

Variations in global temperature and precipitation for the period of 1948 to 2010

Qiaohong Sun · Dongxian Kong · Chiyuan Miao ·
Qingyun Duan · Tiantian Yang · Aizhong Ye ·
Zhenhua Di · Wei Gong

Received: 19 January 2014 / Accepted: 6 May 2014
© Springer International Publishing Switzerland 2014

Abstract Climate change has impacts on both natural and human systems. Accurate information regarding variations in precipitation and temperature is essential for identifying and understanding these potential impacts. This research applied Mann–Kendall, rescaled range analysis and wave transform methods to analyze the trends and periodic properties of global and regional surface air temperature (SAT) and precipitation (PR) over the period of 1948 to 2010. The results show that 65.34 % of the area studied exhibits significant warming trends ($p < 0.05$) while only 3.18 % of the area exhibits significant cooling trends. The greatest warming trends are observed in Antarctica (0.32 °C per decade) and Middle Africa (0.21 °C per decade). Notably, 62.26 % of the area became wetter, while 22.01 % of the area shows drying trends. Northern Europe shows the largest precipitation increase, 12.49 mm per decade. Western Africa shows the fastest drying, −21.05 mm per decade. The rescaled range analysis reveals large areas that show persistent warming trends; this behavior in SAT is more obvious than that in PR. Wave transform results show that a 1-year period of

SAT variation dominates in all regions, while inconsistent 0.5-year bands are observed in East Asia, Middle Africa, and Southeast Asia. In PR, significant power in the wavelet power spectrum at a 1-year period was observed in 17 regions, i.e., in all regions studied except Western Europe, where precipitation is instead characterized by 0.5-year and 0.25-year periods. Overall, the variations in SAT and PR can be consistent with the combined impacts of natural and anthropogenic factors, such as atmospheric concentrations of greenhouse gases, the internal variability of climate system, and volcanic eruptions.

Keywords Global climate change · Mann–Kendall test · Rescaled range analysis · Wave transform

Introduction

It is widely recognized that anthropogenic activities, such as the increasing atmospheric concentrations of carbon dioxide (CO₂) and other greenhouse trace gases, have caused global climate to change. The Fourth Assessment Report of the Intergovernmental Panel on Climate Change (IPCC-AR4) indicates that global mean surface temperatures have risen by 0.74 ± 0.18 °C when estimated by a linear trend over the last 100 years (1906–2005) (Ambenje et al. 2007). Precipitation, another fluctuating quantity, has generally increased over land north of 30° N over the period 1900 to 2005, but downward precipitation trends have been observed in the tropics since the 1970s (Ambenje et al. 2007). Climate change can have major impacts on vulnerable

Q. Sun · D. Kong · C. Miao (✉) · Q. Duan · A. Ye · Z. Di ·
W. Gong
State Key Laboratory of Earth Surface Processes and
Resource Ecology, College of Global Change and Earth
System Science, Beijing Normal University,
Beijing 100875, People's Republic of China
e-mail: miaocy@vip.sina.com

T. Yang
Department of Civil and Environmental Engineering,
University of California,
Irvine, CA 92697, USA

natural systems and sensitive human systems at local, regional, and national scales (Miao et al. 2011a; Miao et al. 2012). The growing concern regarding climate change has heightened the need for accurate information about the space-time distribution of precipitation and temperature (New et al. 2001; Sun et al. 2014).

During the past decades, many parametric and nonparametric techniques for the detection of long-term trends in time series have been developed and applied (Mann 1945; Kendall 1975; Fu and Wang 1992; Miao and Ni 2010; Miao et al. 2010; Wang et al. 2012; Zhang et al. 2012; Abghari et al. 2013). Parametric tests assume that the random variable is normally distributed and homogeneous in variance, while nonparametric tests make no assumptions about the probability distribution (Onoz and Bayazit 2003). Nonparametric tests are more frequently encountered than parametric statistical tests in analysis of hydrometeorological time series (Yue et al. 2002a, b). Various studies have attempted to assess trends in temperature and precipitation changes by using different techniques. Lettenmaier et al. (1994) used a nonparametric seasonal Kendall's test on temperature and precipitation trends in the continental USA over the period 1948–1988. Xu et al. (2003) utilized both a parametric *t* test and nonparametric Mann–Kendall (MK) and Mann–Whitney techniques to detect possible long-term trends in precipitation over Japan. They found that the time series did not exhibit significant evidence of a monotonic trend during the past century. Gemmer et al. (2004) examined monthly precipitation data in China over the period 1951–2002. Partal and Kahya (2006) applied nonparametric methods to estimate the precipitation trend across Turkey during 1929–1993 and identified some significant trends, especially in January, February, and September precipitation and in the annual mean. Alexander et al. (2006) applied Kendall's tau to analyze the global changes in daily climate extremes in temperature and precipitation and found that over 70 % of the global land area sampled showed a significant decrease in the annual occurrence of cold nights and a significant increase in the annual occurrence of warm nights.

Meteorological time series may show periodic cycles in addition to trends (Hsu and Li 2010). The wavelet transform (WT) is a common tool for

analyzing localized power variations within a time series. By decomposing a time series into time-frequency space, one is able to determine both the dominant modes of variability and how those modes vary in time (Torrence and Compo 1998). Wavelet analysis has been successfully applied to detecting climate and hydrology characteristics, such as revealing periodic features of meteorological and hydrological time series. Kim (2004) applied wavelet analysis to estimate the temporal variability of 96 years of precipitation in northern California and found a strong regular decadal oscillation after 1945 with a dominant period of approximately 16 years. Labat (2008) explored a wavelet-based global analysis of discharge fluctuations of 55 large rivers located on five continents and found that large river runoff records are valuable proxies for temperature and precipitation because discharge series integrate intermittent processes over timescales of four or more years. Jiang et al. (2009) used Morlet wavelets to analyze nearly 100 years of a precipitation time series in Northeast China and found periodic oscillations of 2 to 3 years and 5 years.

However, most preexisting studies only focused on single or several regions; few studies have performed comprehensive comparison and analysis of the distribution and characteristics of precipitation and temperature trends on the global scale. Thus, the present study aims (1) to detect the significance and magnitude of the trend of global temperature and precipitation change and (2) to reveal the continuity and periodicity of temperature and precipitation changes in different regions. Potential natural and anthropogenic factors that influence these processes are explored and discussed.

Data and methods

Data

This study uses monthly mean continental surface air temperatures (SAT) at $2.5^\circ \times 2.5^\circ$ resolution from the National Center for Environmental Prediction/National Center for Atmospheric Research (NCEP/NCAR) Global Reanalysis (Kalnay et al. 1996) and monthly mean continental

precipitation (PR) on the same grid from the Global Precipitation Climatology Centre (GPCC) product (Rudolf et al. 2010). The analysis focuses on the period 1948–2010. Because the GPCC dataset does not cover the Antarctic region, the analysis for PR focuses on land outside the Antarctic.

Analysis methods

The statistical significance of trends at each grid point in various regions and globally was tested using the non-parametric Mann–Kendall method (Mann 1945; Kendall 1975), and the magnitude of the trend was computed using Sen’s estimator of slope (Sen 1968). The Morlet wavelet is the most commonly used wavelet for timescale analysis (Kumar and Foufoula-Georgiou 1997) and is preferred when there are periodic or characteristic scales present in the time series (Hsu and Li 2010). Thus, Morlet wavelet analysis (Torrence and Compo 1998) was utilized to estimate the periodicity of precipitation and temperature variations. Moreover, rescaled range analysis (Weron 2002) was applied to calculate the Hurst exponent and reveal the continuity of temperature and precipitation changes.

(a) Mann–Kendall test for monotonic trends

The nonparametric Mann–Kendall statistical test requires sample data to be serially independent. When sample data are serially correlated, the presence of serial correlation in the time series will affect the ability of the test to correctly assess the significance of the trend (Yue and Wang 2004; Yue et al. 2002a, b). Therefore, we adopted the methodology proposed by Yue et al. (2002a, b) to eliminate the autocorrelation of the time series before applying the MK test. The preliminary processes include the following steps:

- 1) Calculating the slope of the trend in the time series using Sen’s estimator as follows (Sen 1968):

$$\beta = \text{Median} \left(\frac{x_j - x_i}{j - i} \right) \tag{1}$$

where the estimator β is the median over all combinations of record pairs for the whole dataset and is thereby resistant to the effect of extreme values in the observations.

- 2) De-trending the time series and dividing the original series into trend series and residual series:

$$x'_t = x_t - T_t = x_t - \beta \times t \tag{2}$$

Calculating the parameters of the autoregressive (AR) model for the residual series:

$$r_k = \frac{\sum_{i=1}^{n-k} (x_i - \bar{x})(x_{i+k} - \bar{x})}{\sum_{i=1}^n (x_i - \bar{x})^2} \tag{3}$$

where n is the length of the time series, r_k is the lag- k autocorrelation efficient, and \bar{x} is the mean. Then, the AR (1) component is removed from the time series using the following equation:

$$x''_t = x'_t - r_1 \times x'_{t-1} \tag{4}$$

Recombining the series after AR component is removed from the trend series:

$$x'''_t = x''_t + T_t \tag{5}$$

where x'''_t is the sample data with the true trend, which is not affected by autocorrelation. Then, the MK test is applied to the new series (x'''_t).

Then, the Mann–Kendall method for testing the statistical significance of trends is given as follows (Mann 1945):

$$Z = \begin{cases} \frac{S-1}{\sqrt{\text{Var}(S)}} & , S > 0 \\ 0 & , S = 0 \\ \frac{S+1}{\sqrt{\text{Var}(S)}} & , S < 0 \end{cases} \tag{6}$$

where

$$S = \sum_{i=1}^{n-1} \sum_{j=i+1}^n \text{sgn}(y_j - y_i) \tag{7}$$

$$\text{sgn}(y_j - y_i) = \begin{cases} 1 & , y_j - y_i > 0 \\ 0 & , y_j - y_i = 0 \\ -1 & , y_j - y_i < 0 \end{cases} \tag{8}$$

$$\text{Var}(S) = \frac{[n(n-1)(2n+5) - \sum_{p=1}^q t_p(t_p-1)(2t_p+5)]}{18} \tag{9}$$

in which y is the new series after eliminating the autocorrelation of the origin time series. y_i and y_j are the

sequential data values at times i and j , respectively, where $j > i$. The number n is the length of time series, q is the number of tied groups, t_p is the p th group and \sum denotes summation over all ties. The null hypothesis (H_0) is accepted if $-Z_{1-a/2} \leq Z \leq Z_{1-a/2}$, where a is the significance level of the test. A typical confidence level of 95 % was used. A positive (negative) value of Z indicates an upward (downward) trend.

The magnitude of the trend is calculated using Sen’s estimator of slope as function (1).

(b) Wavelet transform

The Morlet wavelet is defined as (Torrence and Compo 1998)

$$\psi_0(\eta) = \pi^{-1/4} e^{i\omega_0\eta} e^{-\eta^2/2} \tag{10}$$

where ω_0 is the nondimensional frequency, taken here to be 6 to satisfy the admissibility condition (Farge 1992; Torrence and Compo 1998), and η is dimensionless time. The continuous wavelet transform of x_n with a scaled and translated version of $\psi_0(\eta)$ is

$$W_n(s) = \sum_{n'=0}^{N-1} x_{n'} \psi^* \left[\frac{(n'-n)\delta t}{s} \right] \tag{11}$$

where (*) indicates the complex conjugate, s is the wavelet scale, n is the localized time index, and N is the number of points in the time series. The cone of influence (COI) is here defined as the area in which the wavelet power caused by a discontinuity at the edge drops to e^{-2} of the value at the edge. COI was used to account for the edge effects (Grinsted et al. 2004). The statistical significance of wavelet power can be assessed relative to the null hypotheses that the signal is generated by a stationary process with a given background power spectrum (P_k). The Fourier power spectrum of a first-order autoregressive (AR1) process with lag-1 autocorrelation α is given by (Grinsted et al. 2004)

$$P_k = \frac{1-\alpha^2}{|1-\alpha e^{-2i\pi k}|^2} \tag{12}$$

where k is the Fourier frequency index. Torrence and Compo (1998) use Monte Carlo methods to show that this approximation is very good for the AR1 spectrum. They show that the probability that

the wavelet power of a process with a given power spectrum (P_k) greater than p . The equation is:

$$D \left(\frac{|W_n^X(s)|^2}{\sigma_X^2} < p \right) = \frac{1}{2} P_k \chi_v^2(p) \tag{13}$$

where v is equal to 1 for real wavelets and 2 for complex wavelets. The Morlet wavelet was adapted to analyze the periodic characteristics of SAT and PR.

(c) Rescaled range analysis

The fundamental principle of R/S analysis is given by Weron (2002). The analysis begins with dividing a time series of return of length L into d subseries of length n . For each subseries $m=1, \dots, d$: ① find the mean (E_m) and standard deviation (S_m); ② normalize the data ($Z_{i,m}$) by subtracting the sample mean $x_{i,m} = Z_{i,m} - E_m$ for $i=1, \dots, n$; ③ create a cumulative time series $Y_{i,m} = \sum_{j=1}^i x_{j,m}$ for $i=1, \dots, n$; ④ find the range $R_m = \max\{Y_{1,m}, \dots, Y_{n,m}\} - \min\{Y_{1,m}, \dots, Y_{n,m}\}$; ⑤ rescale the range R_m/S_m . Then, calculate the mean value of the rescaled range for all subseries of length n :

$$(R/S)_n = \frac{1}{d} \sum_{m=1}^d R_m/S_m \tag{14}$$

The R/S statistics asymptotically follow the relation:

$$(R/S)_n \sim cn^H \tag{15}$$

where a Hurst exponent H can be obtained by running the simple linear regression over a sample of increasing time horizons:

$$\log(R/S)_n = \log c + H \log n \tag{16}$$

where the range of H is between 0 and 1, $H=0.5$ suggests a true random walk, $0.5 < H < 1$ indicates “persistent behavior”, and $0 < H < 0.5$ reflects a time series with “anti-persistent behavior.”

Results

Spatial patterns of temperature and precipitation trends

The overall spatial patterns of the annual and seasonal global SAT change are shown in Fig. 1. In annual SAT (including Antarctica), significant warming trends ($p < 0.05$) for the period 1948–2010 occur in 65.34 %

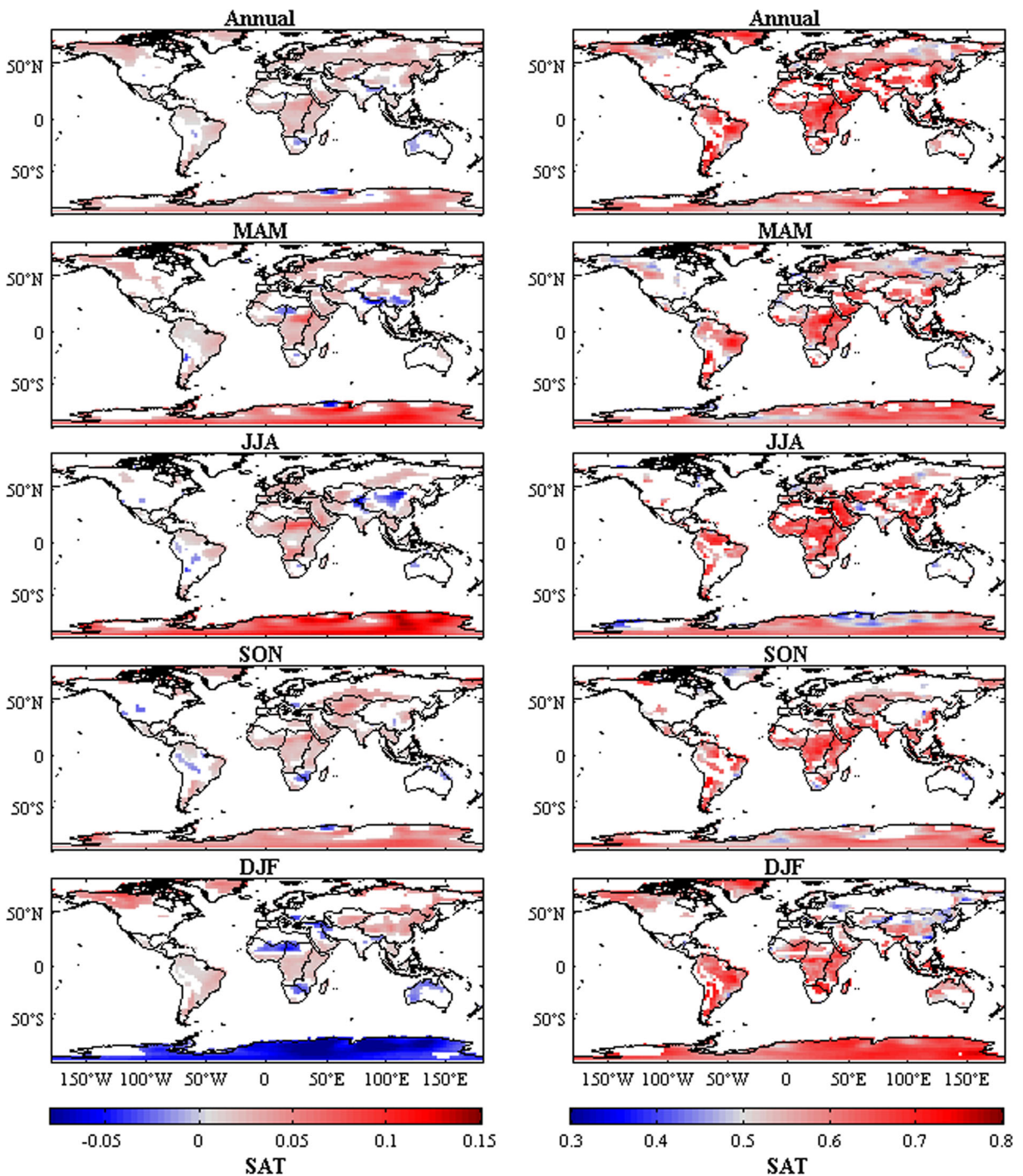


Fig. 1 The distribution map of change trends (*left*) and Hurst exponents (*right*) for annual and seasonal mean temperature during 1948–2010 over the global land. The *blanks* over global land (include Antarctica) indicate there are no significant trends at the 0.05 level

of the area studied. The estimated values of H are in the range of 0.5–1 for most areas (Fig. 1, right), indicating long-term persistence of the warming. This indicates that the warming trends in these areas will very likely

continue in the future. In high-latitude regions, in a few isolated areas such as eastern Russia and northern Antarctica, the values of H are below 0.5, indicating that future values are not dependent on previous values.

On the China-India border, in Western Australia, in southern Africa, and in some isolated areas, the annual mean temperature shows a significant decreasing trend ($p < 0.05$). Only 3.18 % of the area studied shows a significant decreasing trend. Seasonally, significant warming trends are found for all seasons in a large number of grid cells. However, the decreasing trends occur in Southeast Asia and Northern Africa in March, April, and May (MAM). The grid cells in Northwest Africa, southern Africa, and Western Australia have a negative change in December, January, and February (DJF). Exceptionally, significant warming trends are identified for annual mean temperature in MAM, June, July, and August (JJA), and September, October, and November (SON) over Antarctica, while a significant downward trend is discovered in DJF. Moreover, the most distinct warming trend is observed in JJA.

The overall spatial pattern of the precipitation change over global continents (excluding Antarctica) is shown in Fig. 2. The spatial pattern of the precipitation change shows zonal characteristics. Annual precipitation over high-latitude regions in the Northern Hemisphere, Middle Africa, India, and Southeast Asia all increased significantly ($p < 0.05$) during the period 1948–2010. Of the area, 62.26 % became wetter. However, 22.01 % of the area showed negative trends; this area was mainly located at low latitudes, including large areas of South America, southern Africa, Australia, and Indonesia. Some famous dry populated areas in world, such as the Middle East, Middle Asia, became drier and warmer. The value of H in part Middle East is higher than 0.5, but below 0.5 in the rest of Middle Asia, which may indicate different persistent behavior. Seasonally, fewer grids show significant precipitation changes for different seasons. A significant positive trend is found in the high-latitude regions in the Northern Hemisphere, including Russia, Canada, and Greenland, in MAM and DJF. Moreover, distinct downward trends are evident in the east coast of the Gulf of Guinea in MAM, SON, and DJF. In central Australia, significant upward trends are observed in DJF, while for other seasons, precipitation in the region has no significant trend. The seasonal variation in precipitation is not as strong as the seasonal variation in temperature. As Fig. 2 shows, the values of H for the precipitation time series are primarily near 0.5. Thus, persistent behavior for precipitation cannot be observed over large areas.

Trends in regional temperature and precipitation

Figure 3 shows the 5-year-average time series of annual SAT and PR globally and in the Northern and Southern Hemispheres. For SAT, it is obvious that the trends of all three areas are similar: they are all warming. From approximately 1990 to 1995, a slight fluctuation was observed: SAT slightly decreases before warming more rapidly. For PR, the gradual global changes and changes within the Northern Hemisphere are similar, while the precipitation record in the Southern Hemisphere shows more obvious fluctuations.

Figure 4 shows the anomaly relative to the period 1961 to 1990 and the 5-year-average time series of annual mean temperature. Most regions show undulations superimposed on overall rising trends. After the 1990s, SAT rises with an increasing rate. The temperature of East Africa and Middle Africa continued to rise with similar trends. The trends in temperature change over different periods in West Africa and North Africa are largely consistent; the lowest and highest temperatures here occur in 1974 and 2010, respectively. In Asia, all regions except Southeast Asia show brief minima in SAT in the 1970s. Moreover, the temperature changes in Central America and South America are more moderate than those in North America. The temperature changes in Eastern Europe, Northern Europe, and Western Europe are all similar, while Southern Europe shows relatively stable temperatures.

To assess the expected large regional variations in precipitation trends, Fig. 5 shows time series of annual precipitation relative to the period 1961–1990. The variations in precipitation differ over various regions. In Eastern Europe, Middle Africa, South America and North America, the magnitudes of precipitation changes are approximately $-10\sim 10\%$; that is to say, relatively small changes are observed. In Australia, southern Africa, and North Africa, higher annual variations in precipitation are observed, with anomalies of approximately $-20\sim 60\%$.

Table 1 shows the estimates of the trends in annual and seasonal mean temperature change in 19 regions. In most regions, positive trends that are statistically significant at the 0.05 level in annual mean temperature are identified; only four regions satisfy the null hypothesis. The annual mean temperature in Australia and New Zealand shows almost no change. The long-term monotonic trends in mean annual temperature in North Africa, southern Africa, southern Asia, and Australia are weak

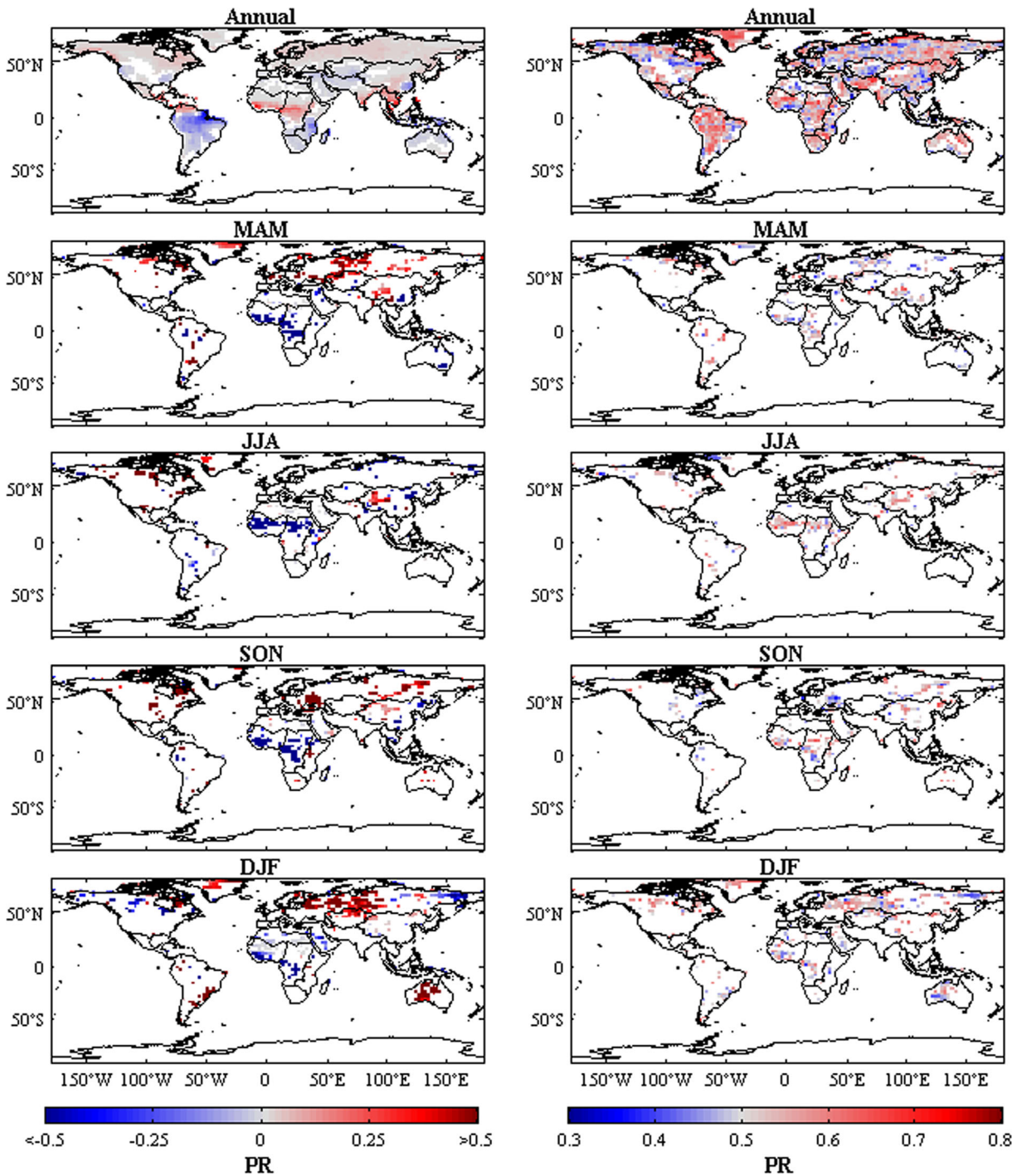


Fig. 2 The distribution of change trends (*left*) and Hurst exponents (*right*) for annual and seasonal precipitation during 1948–2010 over the global land. The *blanks* on global land (exclude Antarctica) indicate there are no significant trends at the 0.05 level

and statistically insignificant. The rate of change in mean annual temperature in regions with significant change varies from 0.07 to 0.32 °C per decade, with

the highest trend estimates observed in Antarctica (0.32 °C per decade) and Middle Africa (0.21 °C per decade). Seasonally, SAT in all seasons has a positive

Fig. 3 The 5-year-average time series of annual mean temperature and precipitation anomalies on globe, Northern Hemisphere, Southern Hemisphere. The baseline is 1961–1990

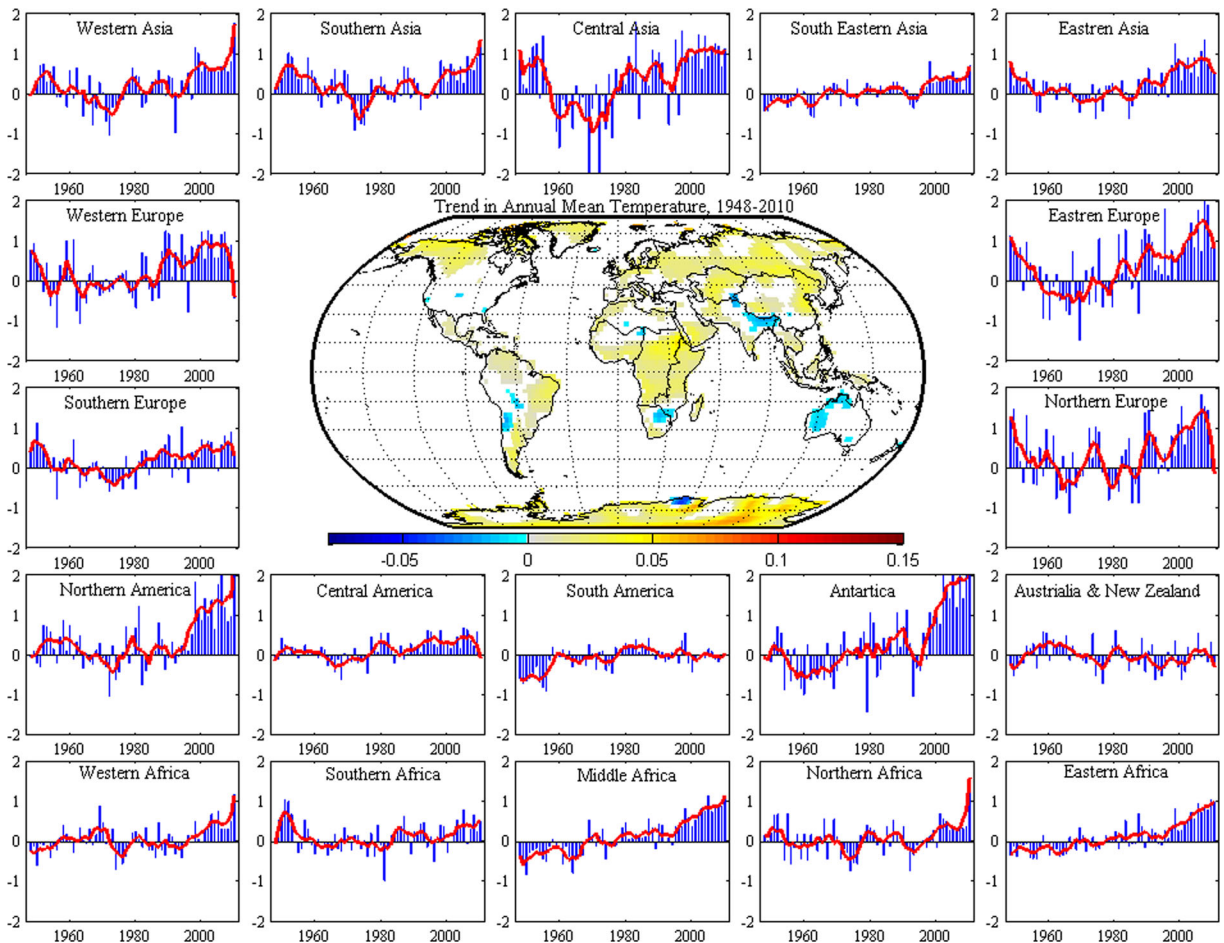
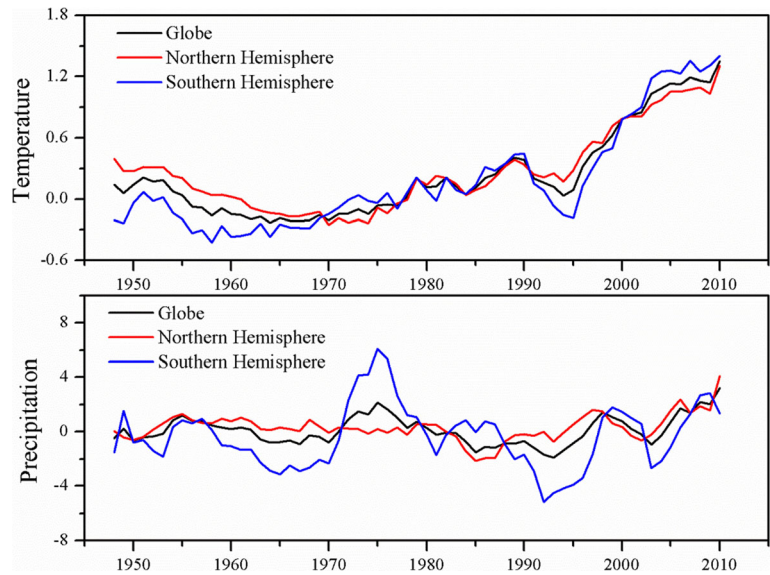


Fig. 4 The time series of annual mean temperature anomalies and 5-year-average series displayed on different regions. The baseline is 1961–1990

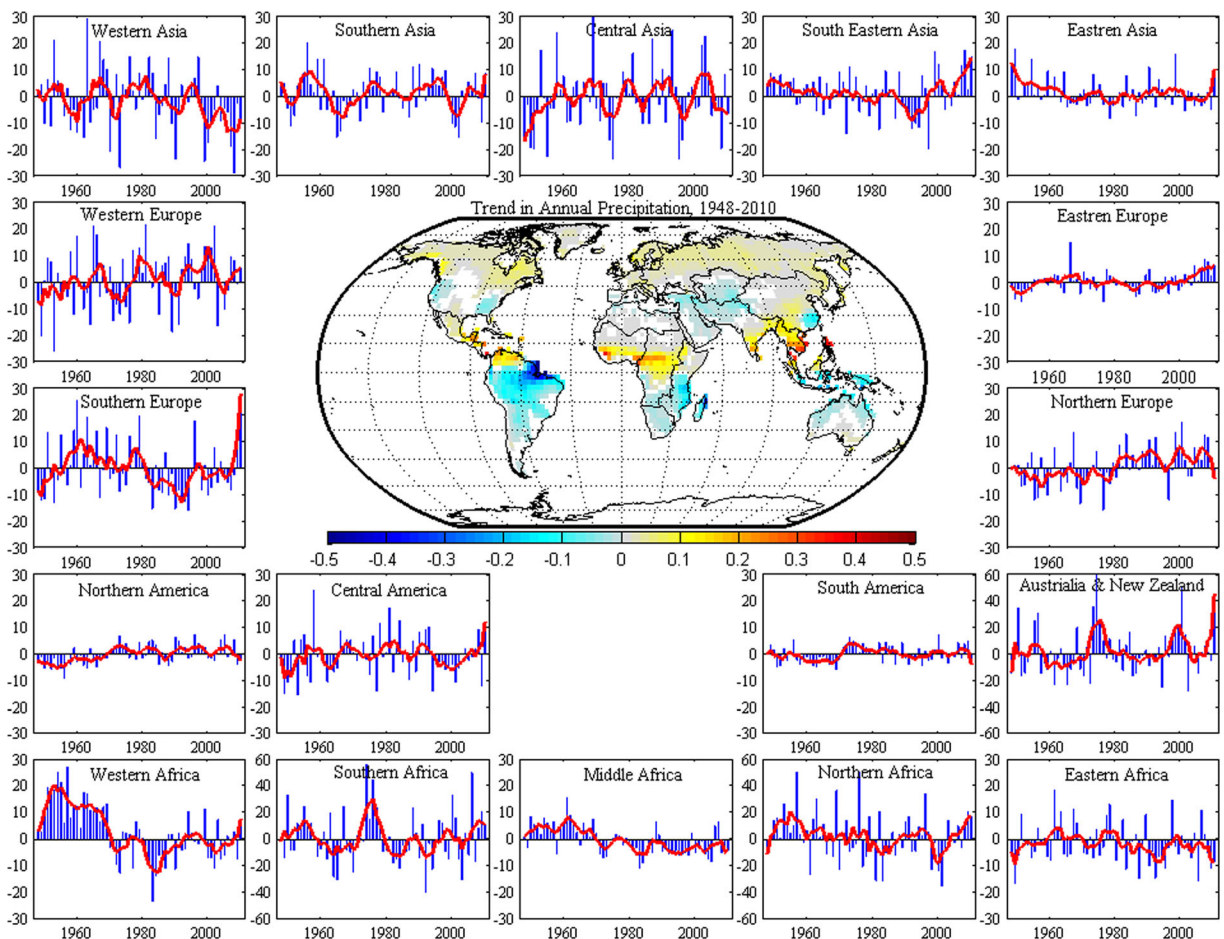


Fig. 5 The time series of annual precipitation anomalies and 5-year-average series displayed on different regions. The baseline is 1961–1990

change for East Africa and Southeast Asia. However, in southern Africa from 1948–2010, significant warming was not observed during all seasons. Other regions show significant trends in different seasons. Significant trends in the mean DJF temperature are observed only in East Asia, East Africa, South America, Southeast Asia, Australia, and New Zealand. Notably, a negative trend is detected in Australia and New Zealand for JJA, with a $-0.07\text{ }^{\circ}\text{C}$ per decade rate of change. For the Hurst exponent of annual mean temperature, regions (except Western Europe) with H values above 0.5 show long-term persistence of warming. In JJA, the values of H in East Asia, Middle Africa, North Africa, Southern Europe, and Western Europe are below 0.5, indicating that future temperatures are independent of previous temperatures.

Table 2 shows estimates of the trends in annual and seasonal precipitation in 18 regions. Over East Africa,

East Asia, Middle Africa, North America, Southeast Asia, southern Africa, South Asia, Southern Europe, West Africa, and Western Asia, the annual precipitation exhibits decreasing trends. Increasing trends are identified for seven other regions. However, analyses of annual precipitation over land indicate that only a few regions have significant trends over the period 1948–2010, including East Africa, Middle Africa, North America, Northern Europe, and West Africa, while the Mann–Kendall test finds that annual precipitation in other regions does not show significant trends. The monotonic trend test indicates that the precipitation in Middle Africa and West Africa tends to decrease at rates of -18.41 and -21.05 mm per decade, respectively. Statistically significant upward trends are observed in Eastern Europe, North America, and Northern Europe; these regions are primarily located at middle and high latitudes. The rate of change (12.49 mm per decade) in

Table 1 The trends slope (β) and Hurst exponent (H) for annual and seasonal mean temperature in different regions

Region	Annual		MAM		JJA		SON		DJF	
	β	H_t	β	H	β	H	β	H	β	H
Western Asia	0.011	0.65	0.014	0.66	0.021	0.68	0.014	0.54	-0.008	0.52
Southern Asia	0.004	0.70	0.003	0.64	0.006	0.65	0.006	0.62	-0.007	0.55
Central Asia	0.020	0.67	0.018	0.58	0.014	0.65	0.034	0.53	0.013	0.52
South Eastern Asia	0.010	0.59	0.005	0.58	0.014	0.56	0.013	0.56	0.007	0.69
Eastern Asia	0.010	0.59	0.015	0.57	-0.002	0.66	0.006	0.58	0.027	0.40
Western Europe	0.015	0.49	0.015	0.43	0.023	0.51	0.005	0.52	0.010	0.44
Eastern Europe	0.020	0.61	0.030	0.57	0.015	0.68	0.020	0.61	0.020	0.44
Southern Europe	0.008	0.63	0.011	0.52	0.021	0.64	0.021	0.53	-0.002	0.46
Northern Europe	0.014	0.62	0.012	0.50	0.010	0.59	0.004	0.59	0.027	0.57
Northern America	0.016	0.65	0.017	0.53	0.003	0.58	0.015	0.64	0.036	0.62
Central America	0.007	0.64	0.010	0.53	0.007	0.56	0.006	0.53	0.006	0.48
South America	0.007	0.67	0.010	0.70	0.004	0.57	0.003	0.51	0.011	0.56
Antarctica	0.032	0.60	0.056	0.60	0.082	0.63	0.038	0.61	-0.048	0.68
Australia & New Zealand	0.00	0.59	0.001	0.51	0	0.50	0	0.53	-0.007	0.54
Western Africa	0.007	0.62	0.007	0.60	0.020	0.61	0.020	0.60	-0.009	0.51
Southern Africa	0.004	0.62	0.003	0.57	0.004	0.56	0.004	0.52	0	0.53
Middle Africa	0.021	0.61	0.025	0.65	0.033	0.64	0.019	0.61	0.005	0.47
Northern Africa	0.005	0.63	0.008	0.61	0.011	0.66	0.009	0.54	-0.005	0.45
Eastern Africa	0.0016	0.57	0.022	0.59	0.015	0.56	0.012	0.58	0.015	0.56

The values with bold font indicate the series has significant change at the 0.05 level

Northern Europe is higher than that of other regions. Table 2 also shows the rate of precipitation change for all seasons over all regions. For JJA, most regions become drier (negative trends), but Central America, North America, Northern Europe, Western Asia, Australia, and New Zealand do not become drier. For SON, wetter trends are observed in many regions, excepting East Asia, Middle Africa, Southeast Asia, and West Africa. Decreases in precipitation are found for all seasons in East Asia and Middle Africa. Precipitation increases in all seasons are found only in Northern Europe. The values of the Hurst exponent of precipitation for almost all regions are in the range of 0.4–0.6. Thus, the persistence or anti-persistence of these time series is not obvious.

WT of temperature and precipitation for all regions

Figure 6 shows the wavelet power spectrum of the monthly mean temperature of 19 critical regions. The wavelet spectrum provides an improved insight into the temporal-scale variability of monthly temperature

series (Labat et al. 2005). From the wavelet power spectrum, the intermittency of each time-scale process can be detected. As expected, these monthly temperature series show significant power at the 1-year period; the annual cyclicality in all regions shows a confidence level greater than 0.95 (Fig. 7). However, the 1-year band of the monthly mean temperature in Middle Africa is not consistent throughout the entire time series: the 95 % confidence regions in the 1-year band disappear during 1948–1953 and reappear after 1953. Moreover, power in the 0.5-year band of the temperature series in East Asia, Middle Africa, and Southeast Asia can be observed, but the 0.5-year bands for these regional temperatures are also not consistent over time. For example, in East Africa, the 95 % confidence region for the 0.5-year band appears relatively consistently only after 1982. On a multi-decadal scale, South Eastern Asia, Middle Africa, and Eastern Africa are characterized by 32-year oscillation (Fig. 7), but the 32-year periods are not over the confidence level of 0.95. Overall, the 1-year period is dominant in all regions.

Table 2 The trends slope (β) and Hurst exponent (H) for annual and seasonal precipitation in different regions

Region	Annual		MAM		JJA		SON		DJF	
	β	H	β	H	β	H	β	H	β	H
Western Asia	-0.3394	0.56	-0.175	0.465	0.019	0.510	0.036	0.571	-0.214	0.52
Southern Asia	-0.007	0.59	-0.012	0.559	-0.157	0.523	0.025	0.533	0.101	0.53
Central Asia	0.187	0.47	-0.197	0.43	-0.086	0.487	0.105	0.492	0.192	0.52
South Eastern Asia	-0.801	0.54	0.209	0.501	-0.337	0.495	-0.253	0.516	-0.32	0.58
Eastern Asia	-0.336	0.48	-0.072	0.476	-0.139	0.449	-0.193	0.460	0.009	0.54
Western Europe	1.017	0.56	0.500	0.568	-0.178	0.380	0.612	0.541	0.109	0.49
Eastern Europe	0.294	0.58	0.154	0.543	-0.070	0.561	0.128	0.564	0.083	0.64
Southern Europe	-0.310	0.56	-0.060	0.477	-0.129	0.493	0.162	0.470	-0.438	0.46
Northern Europe	1.249	0.52	0.294	0.495	0.151	0.467	0.243	0.531	0.52	0.36
Northern America	0.418	0.55	0.324	0.552	0.273	0.495	0.161	0.531	-0.015	0.51
Central America	0.462	0.51	-0.008	0.502	0.240	0.442	0.228	0.427	0.005	0.70
South America	0.413	0.54	0.206	0.565	-0.033	0.471	0.045	0.493	0.216	0.50
Australia & New Zealand	0.849	0.55	-0.008	0.429	0.249	0.417	0.228	0.551	0.759	0.47
Western Africa	-2.105	0.58	-0.335	0.541	-0.909	0.503	-0.694	0.560	-0.093	0.57
Southern Africa	-0.167	0.54	-0.390	0.562	-0.004	0.437	0.107	0.455	0.143	0.54
Middle Africa	-1.841	0.54	-0.497	0.452	-0.406	0.501	-0.509	0.502	-0.185	0.54
Northern Africa	-0.081	0.52	-0.076	0.521	-0.081	0.524	0.009	0.457	-0.097	0.41
Eastern Africa	-0.386	0.52	-0.327	0.484	-0.142	0.508	0.041	0.521	-0.076	0.57

The values with bold font indicate the series has significant change at the 0.05 level

Figure 8 shows the wavelet power spectrum of the precipitation time series of 18 regions. Most regions show significant power at the 1-year period; however, Western Europe does not. Over Western Europe, the 1-year period is not significant at the 95 % confidence level (Fig. 9), but 95 %-significant regions can be observed, though they are distributed sporadically, in the 0.5- and 0.25-year bands. Over Central America, East Africa, East Asia, Eastern Europe, North America, South America, Southeast Asia, southern Africa, South Asia, and West Africa, significance in the 1-year band of the monthly precipitation is consistent throughout the entire time series. The continuous wavelet power spectrum for Australia shows high wavelet power in the 1-year band in 1951–1968, 1970–1982, and 1984–2010. The precipitation series of Northern Europe has high power in the 1-year band during 1948–1990, while 95 %-confident regions in the 1-year band appear only sporadically after 1990. As for Central Asia and Southern Europe, regions of 95 % confidence in the 1-year band are distributed sporadically throughout the entire period; the 1-year period dominates. A significant wavelet variance in the 0.5-year band can be observed

over Central Asia, Australia, Central America, Middle Africa, South Asia, Southern Europe, Western Asia, and Western Europe, but the regions of significance are distributed more sporadically than are the 1-year regions of significance. Only over Middle Africa and South Asia are the regions of 95 % confidence distributed relatively consistently. On interannual scales, Central Asia, Western Europe, and Middle Africa show 6–7-year fluctuations; Central Asia also is characterized by 12-year fluctuation. Sixteen- to eighteen-year periodicities are showed in Western Europe and Northern Africa. However, these periodicities are not over the confidence level of 0.95.

Discussion and summary

A number of factors may be affecting the results. The first potential factor is the length of the time series. Yue et al. (2002a, b) revealed that the sample size affects the ability of the Mann–Kendall test to detect monotonic trends: as the sample size increases, the tests become more powerful; therefore, that wavelet analysis may

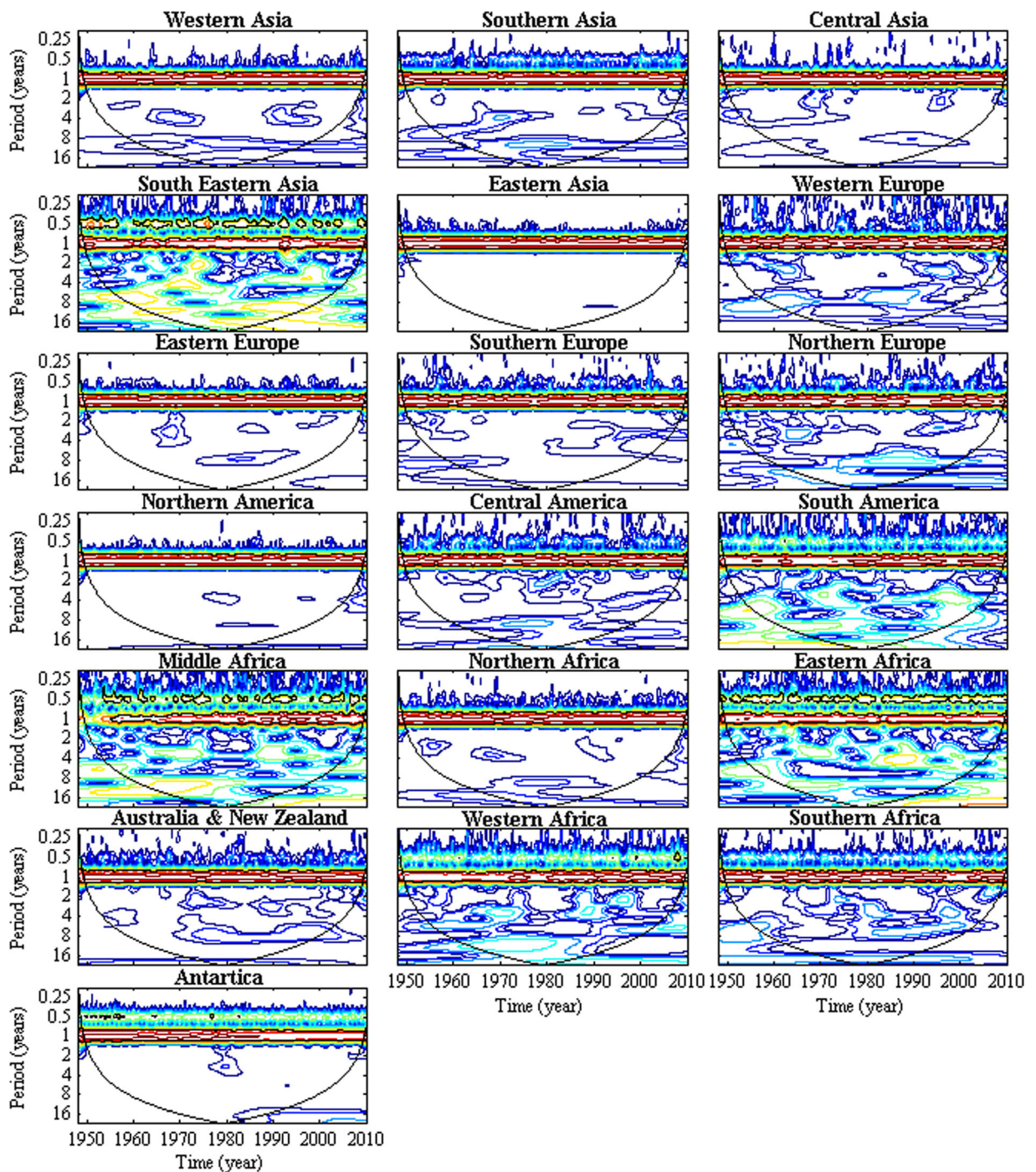


Fig. 6 Wavelet power spectrum of monthly mean temperature for 19 regions

reveal more information for longer time series. Thus, more meaningful and accurate results may be obtained if there are longer time series.

Secondly, the changes in SAT and PR over the twentieth century observed in the study are consistent with the

combined impacts of natural and anthropogenic forcings (Tett et al. 1999; Stott 2000; Miao et al. 2011b; Miao et al. 2013). It is well known that human activity is perturbing the chemical composition and radiative balance of the Earth’s atmosphere (McCormick et al. 1995). The

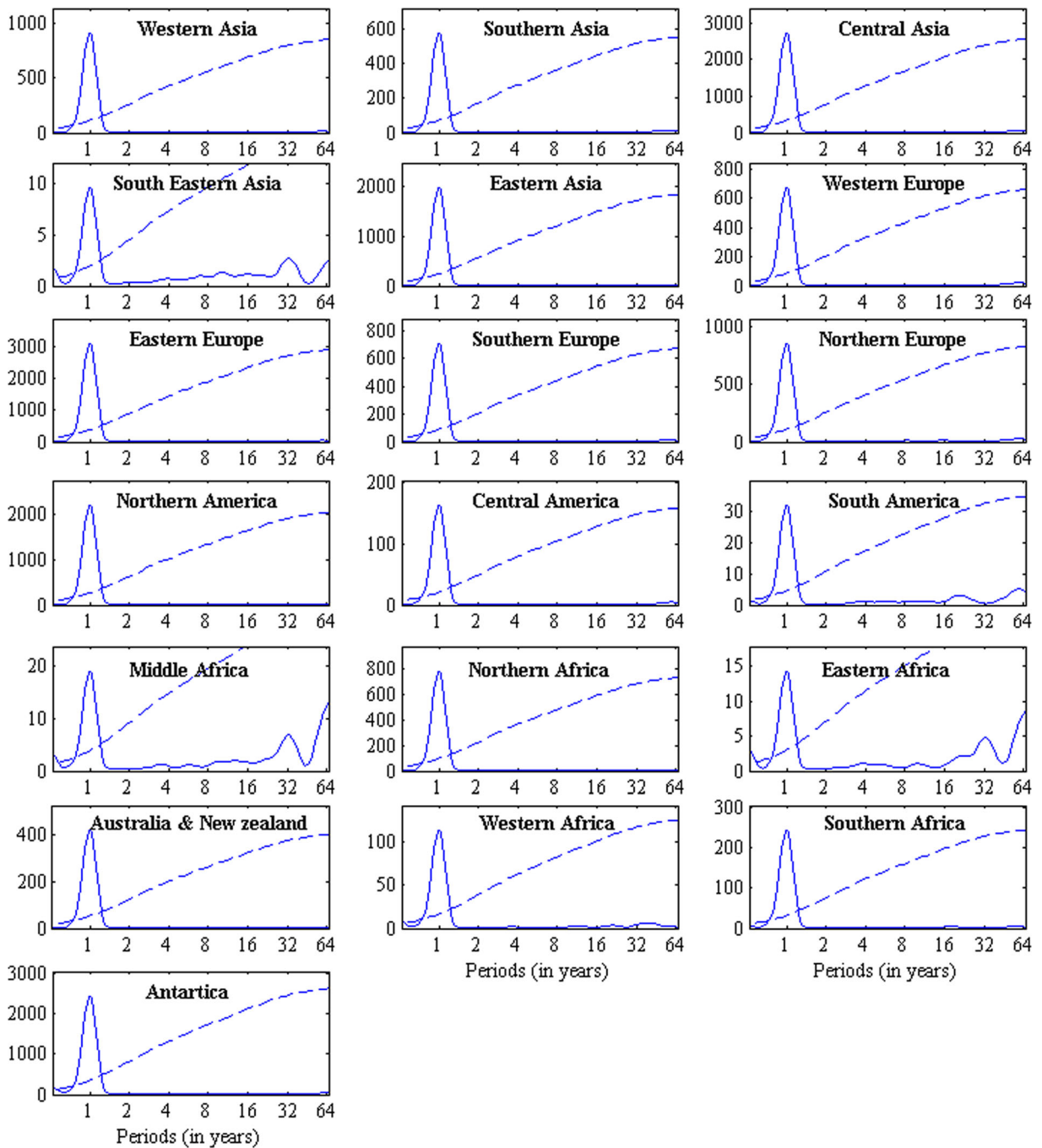


Fig. 7 The global wavelet spectrum of monthly temperature in 19 regions in 95 % confidence interval (*dotted lines*)

warming trend over global land, as Figs. 3 and 4 show, was likely due to increasing atmospheric concentrations of greenhouse gases (CO₂, CH₄, N₂O, etc.) from anthropogenic activities. Of these greenhouse gases, increases in CO₂ are responsible for the largest forcing (Forster et al. 2007). For the decade from 1995 to 2005, the

growth rate of CO₂ in the atmosphere was 1.9 ppm per year and the CO₂ radiative forcing (RF) increased by 20 %; this is the largest change observed or inferred for any decade in at least the last 200 years (Forster et al. 2007). Thus, it is obvious that SAT over global land has been warming more rapidly since 1995 (Figs. 3 and 4).

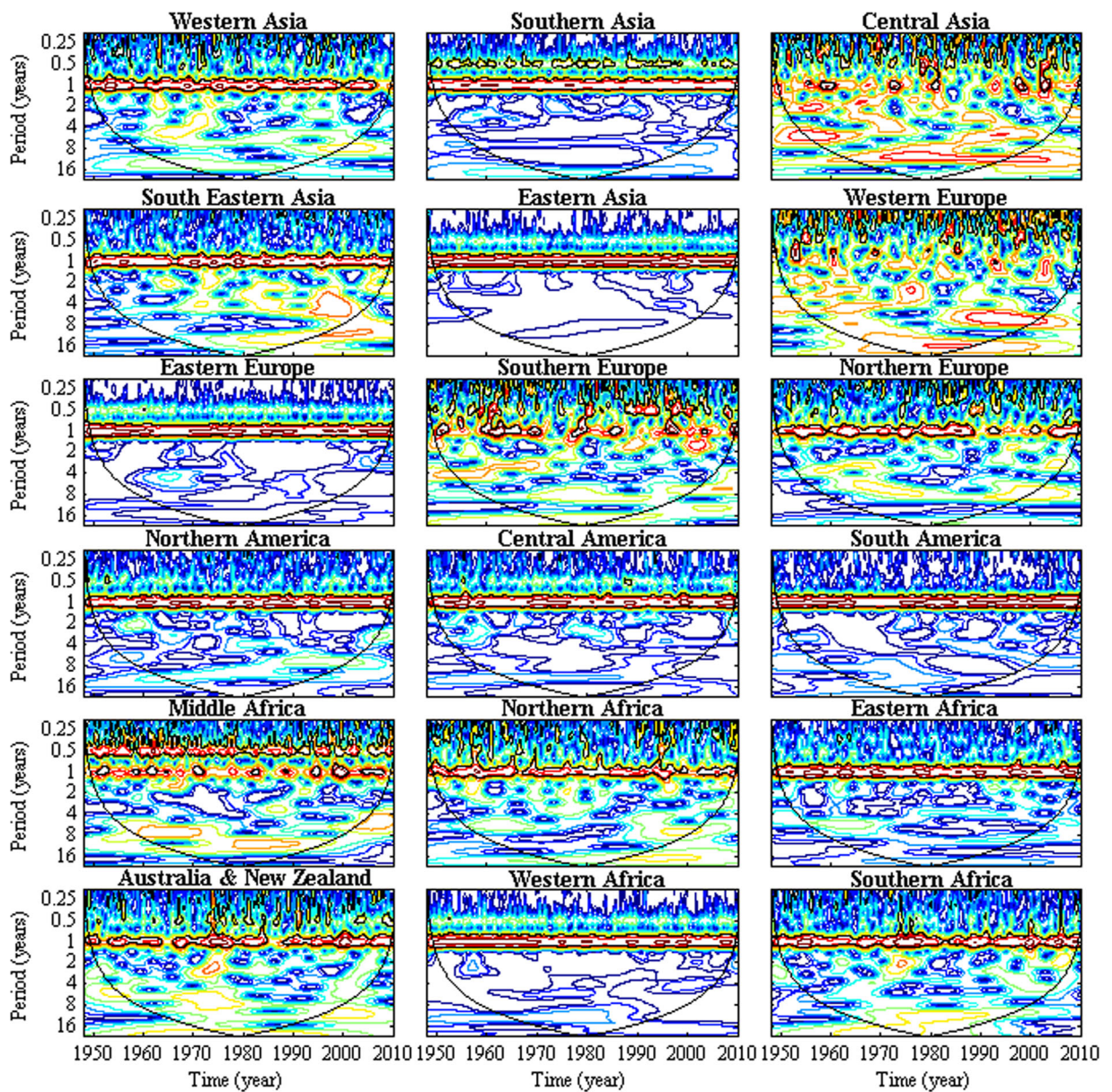


Fig. 8 Wavelet power spectrum of monthly precipitation for 18 regions

Natural forcings and the internal variability of the climate system itself are both important in the change of SAT and PR. The El Niño-Southern Oscillation (ENSO) affects the dominant mode of variability in global and hemispheric land precipitation, and the Arctic and Antarctic Oscillation (AO and AAO) most likely affect precipitation changes in mid- and high latitudes (New et al. 2001). The drying trends observed in southern Africa, Northern Australia, Central and West Asia, and parts of southeast of China and the USA, as

Fig. 1 shows, may be related to the internal variability of the climate system. The results that significant warming trends over Antarctica are identified in MAM, JJA and SON but not in DJF (Fig. 1), which is consistent with the findings of Gong (1999). Gong (1999) shows that the downward trend in the DJF average temperature is likely related to the strengthening of the Antarctic oscillation. Similarly, the observed positive trends in wintertime temperatures over Europe, drying trends over Southern Europe (Figs. 1, 3, and 4; Table 2) and significant

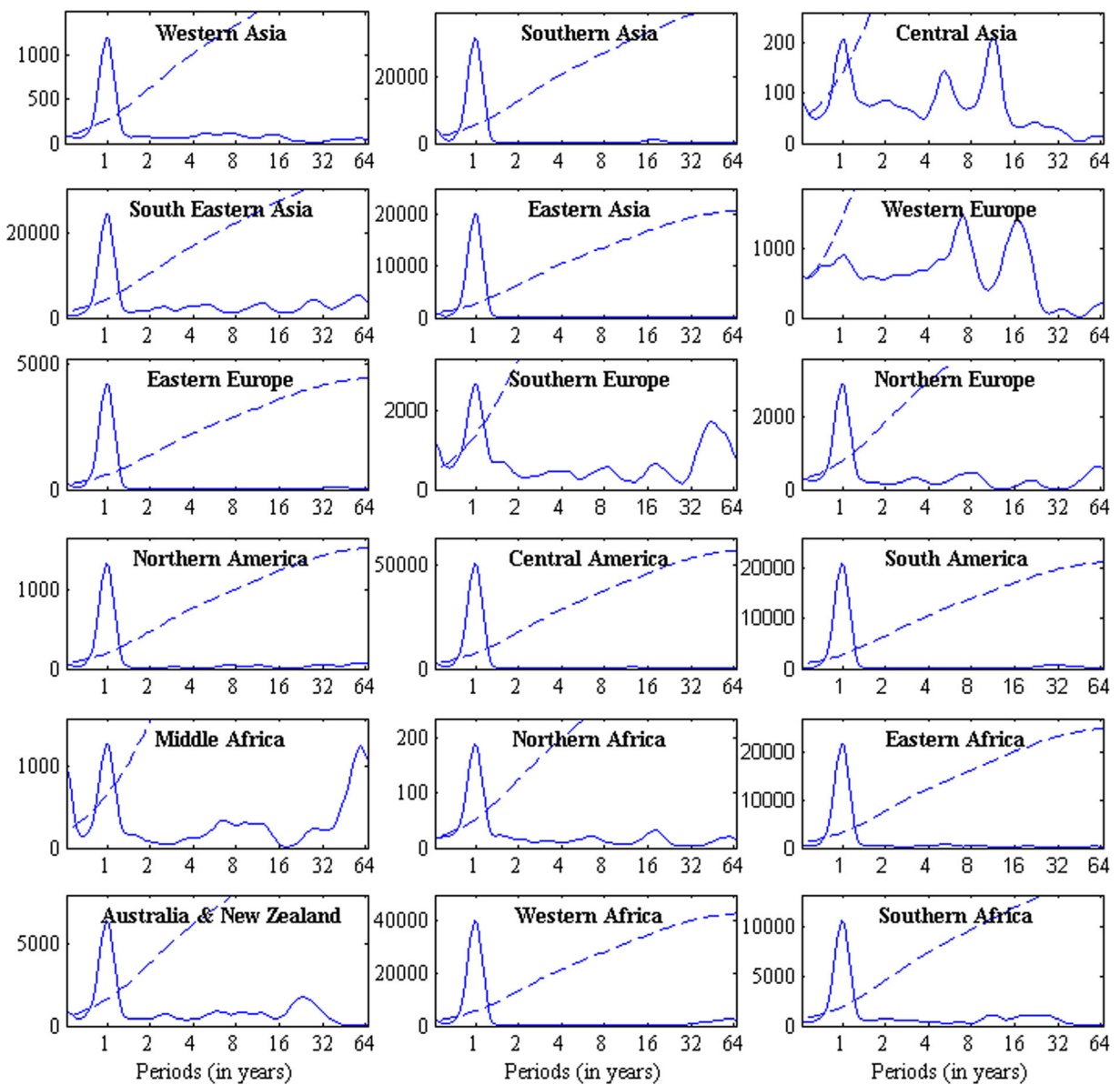


Fig. 9 The global wavelet spectrum of monthly precipitation in 18 regions in 95 % confidence interval (*dotted lines*)

wetting trends over Northern Europe (Table 2) are linked to the North Atlantic Oscillation (NAO) (Hurrell and Loon 1997). Figure 5 shows that Southern Europe become drier while Northern Europe became wetter since 1980. The results may be due in part to the NAO, which has tended to remain in one phase since 1980 (Hurrell and Loon 1997).

Volcanic eruptions are an important natural cause of climate change on many timescales (Robock 2000; Robock and Mao 1995). Volcanic aerosols scatter incoming solar radiation to space, increasing planetary

albedo and cooling the earth’s surface and troposphere (Robock and Mao 1995). Modest cooling ($\sim 0.1\text{--}0.2\text{ }^\circ\text{C}$) is observed for 1 to 2 years after these large events (Mass and Portman 1989). The global and regional SAT experienced a distinctive cooling period in the early 1990s (Figs. 3 and 4), which may be the result of the eruption of Mt. Pinatubo in 1991 (McCormick et al. 1995; Xiao and Li 2011).

In conclusion, in this study, several techniques are applied to analyze the long-term trends in time series of global and regional temperature and precipitation. On

the spatial scale, for SAT, application of the Mann–Kendall test for annual and seasonal mean temperature and time series shows that significant warming trends ($p < 0.05$) for the period 1948–2010 occur over 65.34 % of land, while cooling trends are observed in only 3.18 % of the area. From the results of R/S, large areas show persistent warming trends. Over Antarctica, significant warming trends are identified in the mean temperature in MAM, JJA, and SON, but not in DJF. For PR, at middle and higher latitudes, significant upward trends are observed. Approximately 62.26 % of areas become wetter. Significant downward trends are observed in 22.01 % of the area studied; these areas are mainly in southern Africa, Northern Australia, Central and West Asia, parts of southeast China, and the USA. The regional average temperature and precipitation are also analyzed. For SAT, results indicate that most regions show undulating rising trends overall, with SAT rising at a faster rate after the 1990s. The results of the Mann–Kendall test identify statistically significant increasing trends in annual mean temperature and mean temperature at the 0.05 level in MAM, JJA, and SON; the rates of change vary from 0.07 to 0.21 °C per decade. Furthermore, results from the wavelet analysis of monthly mean temperature show that the 1-year period dominates in all regions. Only in East Asia, Middle Africa, and Southeast Asia are inconsistent 0.5-year bands observed.

For PR, the magnitudes of the anomalies are approximately –20~60 % in Australia, southern Africa, and Northern Africa, while in other regions they are approximately –30~30 %, and relatively stable changes are observed. The monotonic trend test for annual precipitation indicates that precipitation in Middle Africa and Western Africa is decreasing; statistically significant increases are observed only in Eastern Europe, North America, and Northern Europe. Significant power in the wavelet power spectrum at the 1-year period was observed in 17 regions, but was absent in Western Europe, where the precipitation is characterized by 0.5- and 0.25-year periods. Unlike the periodic properties of temperature, for precipitation, the 1-year band is not consistent throughout the entire time series. The results from R/S show that persistent behaviors in SAT are more obvious than in PR.

Acknowledgments Funding for this research was provided by the National Natural Science Foundation of China (no. 41001153), the State Key Laboratory of Earth Surface Processes and Resource

Ecology, and Fundamental Research Funds for Central Universities. Thanks are also expressed to the National Center for Environmental Prediction/National Center for Atmospheric Research (NCEP/NCAR) and the Global Precipitation Climatology Centre (GPCC) for permission to access the climate data.

References

- Abghari, H., Tabari, H., & Talaei, P. H. (2013). River flow trends in the west of Iran during the past 40 years: impact of precipitation variability. *Global and Planetary Change, 101*, 52–60.
- Alexander, L. V., Zhang, X., Peterson, T. C., Caesar, J., Gleason, B., Tank, A. M. G. K., et al. (2006). Global observed changes in daily climate extremes of temperature and precipitation. *Journal of Geophysical Research, 111*, D05109. doi:10.1029/2005jd006290.
- Ambenje, P., et al. (2007). In S. Solomon, D. Qin, M. Manning, Z. Chen, M. Marquis, K. B. Averyt, M. Tignor, & H. L. Miller (Eds.), *IPCC, 2007: climate change 2007: the scientific basis. Contribution of working group I to the fourth assessment report of the inter-governmental panel on climate change* (p. 243). Cambridge: Cambridge University Press.
- Farge, M. (1992). Wavelet transforms and their applications to turbulence. *Annual Review of Fluid Mechanics, 24*, 395–458.
- Forster, P., et al. (2007). In S. Solomon, D. Qin, M. Manning, Z. Chen, M. Marquis, K. B. Averyt, M. Tignor, & H. L. Miller (Eds.), *Changes in atmospheric constituents and in radiative forcing. Climate change 2007: the physical science basis. Contribution of working group I to the fourth assessment report of the intergovernmental panel on climate change*. Cambridge: Cambridge University Press.
- Fu, C., & Wang, Q. (1992). The definition and detection of the abrupt climate change. *Scientia Atmospherica Sinica, 16*, 482–493.
- Gemmer, M., Becker, S., & Jiang, T. (2004). Observed monthly precipitation trends in China 1951–2002. *Theoretical and Applied Climatology, 77*(1–2), 39–45.
- Gong, D. (1999). Antarctic climate change under the background of global warming. *Scientia Geographica Sinica, 19*, 102–107.
- Grinsted, A., Moore, J. C., & Jevrejeva, S. (2004). Application of the cross wavelet transform and wavelet coherence to geophysical time series. *Nonlinear Processes in Geophysics, 11*, 561–566.
- Hsu, K. C., & Li, S. T. (2010). Clustering spatial–temporal precipitation data using wavelet transform and self-organizing map neural network. *Advances in Water Resources, 33*(2), 190–200.
- Hurrell, J., & Loon, H. V. (1997). Decadal variations in climate associated with the North Atlantic Oscillation. *Climatic Change, 36*, 301–326.
- Jiang, X., Liu, S. H., Ma, M. M., Zhang, J., & Song, J. (2009). A wavelet analysis of the precipitation time series Northeast China during the last 100 years. *Geographical Research, 28*, 354–362.
- Kalnay, E., Kanamitsu, M., & Kistler, R. (1996). The NCEP/NCAR 40-year reanalysis project. *Bulletin of the American Meteorological Society, 77*, 437–471.

- Kendall, M. G. (1975). *Rank correlation methods*. London: Charles Griffin.
- Kim, S. (2004). Wavelet analysis of precipitation variability in northern California, U.S.A. *KSCCE Journal of Civil Engineering*, 8(4), 471–477.
- Kumar, P., & Foufoula-Georgiou, E. (1997). Wavelet analysis for geophysical applications. *Reviews of Geophysics*, 35(4), 385.
- Labat, D. (2008). Wavelet analysis of the annual discharge records of the world's largest rivers. *Advances in Water Resources*, 31(1), 109–117.
- Labat, D., Ronchail, J., & Guyot, J. L. (2005). Recent advances in wavelet analyses: part 2—Amazon, Parana, Orinoco and Congo discharges time scale variability. *Journal of Hydrology*, 314, 289–311.
- Lettenmaier, D. P., Wood, E. F., & Wallis, J. R. (1994). Hydro-climatological trends in the continental United States, 1948–88. *Journal of Climate*, 7, 586–607.
- Mann, H. B. (1945). Nonparametric tests against trend. *Econometrica*, 13, 245–259.
- Mass, C. F., & Portman, D. A. (1989). Major volcanic eruptions and climate: a critical evaluation. *Journal of Climate*, 2(6), 566–593.
- Mccormick, M. P., Thomason, L. W., & Trepte, C. R. (1995). Atmospheric effects of the Mt Pinatubo eruption. *Nature*, 373(6513), 399–404.
- Miao, C. Y., & Ni, J. R. (2010). Implement of filter to remove the autocorrelation's influence on the Mann-Kendall test: a case in hydrological series. *International Journal of Food Agriculture & Environment*, 8(3), 1241–1246.
- Miao, C. Y., Ni, J. R., & Borthwick, A. G. L. (2010). Recent changes in water discharge and sediment load of the Yellow River basin, China. *Progress in Physical Geography*, 34(4), 541–561.
- Miao, C. Y., Ni, J. R., Borthwick, A. G. L., & Yang, L. (2011a). A preliminary estimate of human and natural contributions to the changes in water discharge and sediment load in the Yellow River. *Global and Planetary Change*, 76(3–4), 196–205.
- Miao, C. Y., Yang, L., & Li, S. L. (2011b). Streamflow changes and its influencing factors in the mainstream of the Songhua River basin, Northeast China over the past 50 years. *Environmental Earth Science*, 63(3), 489–499.
- Miao, C. Y., Duan, Q. Y., Yang, L., & Borthwick, A. G. L. (2012). On the applicability of temperature and precipitation data from CMIP3 for China. *Plos One*, 7(9), e44659. doi:10.1371/journal.pone.0044659.
- Miao, C. Y., Duan, Q. Y., Sun, Q. H., & Li, J. D. (2013). Evaluation and application of Bayesian multi-model estimation in temperature simulations. *Progress in Physical Geography*, 37(6), 727–744.
- New, M., Todd, M., Hulme, M., & Jones, P. (2001). Precipitation measurements and trends in the twentieth century. *International Journal of Climatology*, 21(15), 1889–1922.
- Onoz, B., & Bayazit, M. (2003). The power of statistical tests for trend detection. *Turkish Journal of Engineering and Environmental Sciences*, 27(4), 247–251.
- Partal, T., & Kahya, E. (2006). Trend analysis in Turkish precipitation data. *Hydrological Processes*, 20(9), 2011–2026.
- Robock, A. (2000). Volcanic eruptions and climate. *Reviews of Geophysics*, 38(2), 191–219.
- Robock, A., & Mao, J. (1995). The volcanic signal in surface temperature observations. *Journal of Climate*, 8, 1086–1103.
- Rudolf B., Becker A., Schneider U., Meyer-Chiristoffer A., & Ziese M. (2010). The new “GPCC Full Data Reanalysis Version 5” providing high-quality gridded monthly precipitation data for the global land-surface is public available since December. GPCC Status Rep, 2010.
- Sen, P. K. (1968). Estimates of the regression coefficient based on Kendall's tau. *Journal of the American Statistical Association*, 63, 1379–1389.
- Stott, P. A. (2000). External control of 20th century temperature by natural and anthropogenic forcings. *Science*, 290(5499), 2133–2137.
- Sun, Q. H., Miao, C. Y., Duan, Q. Y., Kong, D. X., Ye, A. Z., Di, Z. H., et al. (2014). Would the ‘real’ observed dataset stand up? A critical examination of eight observed gridded climate datasets for China. *Environmental Research Letters*, 9(1), 015001. doi:10.1088/1748-9326/9/1/015001.
- Tett, S. F. B., Stott, P. A., Allen, M. R., Ingram, W. J., & Mitchell, J. F. B. (1999). Causes of twentieth-century temperature change near the Earth's surface. *Nature*, 399, 569–572.
- Torrence, C., & Compo, G. P. (1998). A practical guide to wavelet analysis. *Bulletin of the American Meteorological Society*, 79, 61–78.
- Wang, Q. X., Fan, X. H., Qin, Z. D., & Wang, M. B. (2012). Change trends of temperature and precipitation in the Loess Plateau Region of China, 1961–2010. *Global and Planetary Change*, 92–93, 138–147.
- Weron, R. (2002). Estimating long range dependence: finite sample properties and confidence intervals. *Physica A: Statistical Mechanics and its Applications*, 312, 285–299.
- Xiao, D., & Li, J. (2011). Mechanism of stratospheric decadal abrupt cooling in the early 1990s as influenced by the Pinatubo eruption. *Chinese Science Bulletin*, 56(8), 772–780.
- Xu, Z. X., Takeuchi, K., & Ishidaira, H. (2003). Monotonic trend and step changes in Japanese precipitation. *Journal of Hydrology*, 279(1–4), 144–150.
- Yue, S., & Wang, C. (2004). The Mann-Kendall test modified by effective sample size to detect trend in serially correlated hydrological series. *Water Resources Management*, 18, 201–218.
- Yue, S., Pilon, P., Phinney, B., & Cavadias, G. (2002a). The influence of autocorrelation on the ability to detect trend in hydrological series. *Hydrological Processes*, 16(9), 1807–1829.
- Yue, S., Pilon, P., & Cavadias, G. (2002b). Power of the Mann-Kendall and Spearman's rho tests for detecting monotonic trends in hydrological series. *Journal of Hydrology*, 259(1–4), 254–271.
- Zhang, Q., Sun, P., Singh, V. P., & Chen, X. (2012). Spatial-temporal precipitation changes (1956–2000) and their implications for agriculture in China. *Global and Planetary Change*, 82–83, 86–95.